Crack initiation at thin-film edges with weak singularity

L.Y. Shang [a], Z.L. Zhang [b] and B. Skallerud [c]

Department of Structural Engineering, Norwegian University of Science and Technology (NTNU), N-7491 Trondheim, Norway

[a]lingyun.shang@hotmail.com, [b]zhiliang.zhang@ntnu.no, [c]bjorn.skallerud@ntnu.no

Keywords: fracture mechanics, stress intensity factor, weak singularity, free edge, MEMS

Abstract. This paper concentrates on the singular stress fields at free edges in multi-layered structures. A path independent contour integral method is employed to calculate the intensity of the singular stress fields. The computational procedure is also demonstrated in a flow chart. To provide application guidance for engineers, standardized numerical formulae for normalized stress intensity factors are summarized corresponding to different material combinations. The effect of the bond width, the thickness of the metal layer and the material elasticity on the stress intensity factor are then quantified. Anisotropy of the single crystal silicon is addressed. Furthermore, applicability of the proposed approach is stated and the valid range of the *K*-dominated field is also presented. Results obtained from the H-integral approach are in good agreement with those obtained from the detailed finite element solutions.

Introduction

With the development of micromachining techniques, multi-layered thin films on silicon substrates have a wide variety of applications in electronics packaging and integrated circuits. Due to the elastic mismatch, stress concentrations may develop and a weak singularity (λ>0.9) may exist at free edges (Fig. 1). The initiation of failure at free edges in multi-material systems often occurs. Hence, to characterize the singular stress fields at these failure sites becomes a critical issue. It is well known that the interface stress fields around the notch tip are of the form $K_m^n r^{\lambda_m - 1} \left(m = 1, 2, \cdots N \right)$ where N is the number of eigenvalues available from the characteristic equation, r is the radial distance from the interface corner and K_m^n is the intensity of the singular stress fields. $\lambda_m - 1$ is the order of the stress singularity, depending on the material elastic properties and joint geometries described by angles α and β. In addition to these parameters, the stress intensity factor K_m^n depends on the remote loading. The stress field is singular for $0 < \lambda_m < 1$. The knowledge of both K_m^n and λ_m are needed to fully describe the singular stresses and displacements in the vicinity of the notch tip.

Over the past four decades, the order of the stress singularity, the near-tip fields, the methods to evaluate the stress intensity factor for a general corner, and corresponding failure criteria have been extensively investigated. Nevertheless, little attention [1-3] has been given to assess the weak singular stress fields at free edges for minimizing risk of failure in multi-layered structures.

Theory

An efficient computational procedure to obtain the stress intensity factor around a bi-material interface corner is briefly described herein, see also the flow chart (Fig. 2). The detailed representations can be found elsewhere [4, 5].

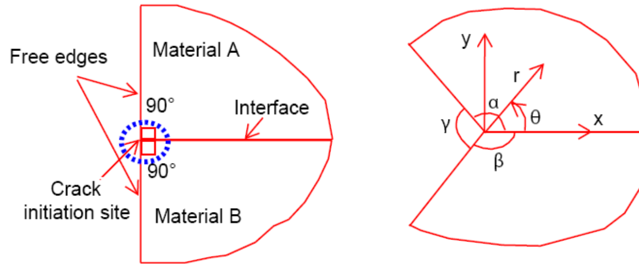

Fig. 1 An edge geometry with dissimilar materials

Asymptotic analysis

Asymptotic analysis can be performed to compute the displacements and stresses at the bi-material interface corner. Two eigenvalue problems are solved on a basis of Stroh's sextic formalism [6-8] and Williams' eigenfunction expansion method [9].

The first eigenvalue problem is material-related and can be obtained by means of displacement **u** (1) and stress function **φ** (2) combined with the constitutive law and equilibrium equations.

$$\mathbf{u} = \sum_{\alpha=1}^{3}\left[\mathbf{a}_\alpha f_\alpha(z_\alpha) + \bar{\mathbf{a}}_\alpha f_{\alpha+3}(\bar{z}_\alpha)\right],\ \alpha = 1,2,3\,, \tag{1}$$

$$\boldsymbol{\varphi} = \sum_{\alpha=1}^{3}\left[\mathbf{b}_\alpha f_\alpha(z_\alpha) + \bar{\mathbf{b}}_\alpha f_{\alpha+3}(\bar{z}_\alpha)\right],\ \alpha = 1,2,3\,. \tag{2}$$

f_α are arbitrary functions of the arguments z_α, where $z_\alpha = x + p_\alpha y$ is the complex variable. The six complex eigenvalues p_α satisfy $p_{\alpha+3} = \bar{p}_\alpha$ and **a**, **b** are the Stroh eigenvectors.

The second eigenvalue problem is geometry-related and can be solved by applying the boundary conditions (3) for the interface notch problem [10], see Fig. 1.

$$\mathbf{t}^A(\alpha) = 0\ ,\ \mathbf{t}^B(-\beta) = 0\ ,\ \mathbf{t}^A(0) = \mathbf{t}^B(0)\ ,\ \mathbf{u}^A(0) = \mathbf{u}^B(0)\,. \tag{3}$$

Path independent H-integral approach

In traditional fracture mechanics, K is a dominant coefficient to describe the crack tip conditions and define the amplitude of crack tip singularity. In a manner similar to K, the term H is employed herein to characterize the intensity of singular stress field for a notched body without a preexisting crack. Based on Betti's reciprocal work theorem [11], the H-integral approach is one of the most powerful approaches using finite element results to obtain stress intensities for configurations with cracks or notches. Choosing $f(z_\alpha)$ [6, 7, 12] as

$$f_\alpha(z_\alpha) = \frac{1}{\lambda} z_\alpha^\lambda q_\alpha \ \text{ and } \ f_{\alpha+3}(\bar{z}_\alpha) = \frac{1}{\lambda}\bar{z}_\alpha^\lambda h_\alpha\,, \tag{4}$$

and utilizing normalizations of the mode I fields by $\sigma_{22}(\theta=0) = K_I^n r^{\lambda_I - 1}$ and of the mode II fields by $\sigma_{12}(\theta=0) = K_{II}^n r^{\lambda_{II}-1}$, the inplane asymptotic fields surrounding the notch tip can be expressed as:

$$\begin{aligned} \sigma_{ij}^M(r,\theta) &= K_I^n r^{\lambda_I - 1} f_{ij}^{IM}(\theta) + K_{II}^n r^{\lambda_{II}-1} f_{ij}^{IIM}(\theta) \\ u_i^M(r,\theta) &= K_I^n r^{\lambda_I} g_i^{IM}(\theta) + K_{II}^n r^{\lambda_{II}} g_i^{IIM}(\theta) \end{aligned}\ , \tag{5}$$

here M corresponds to material A or B, see Fig. 1. In the absence of body forces, the H-integral takes the form [4]:

$$H = \int_\Gamma \left(\sigma_{ij} u_i^* - \sigma_{ij}^* u_i\right) n_j ds\,, \tag{6}$$

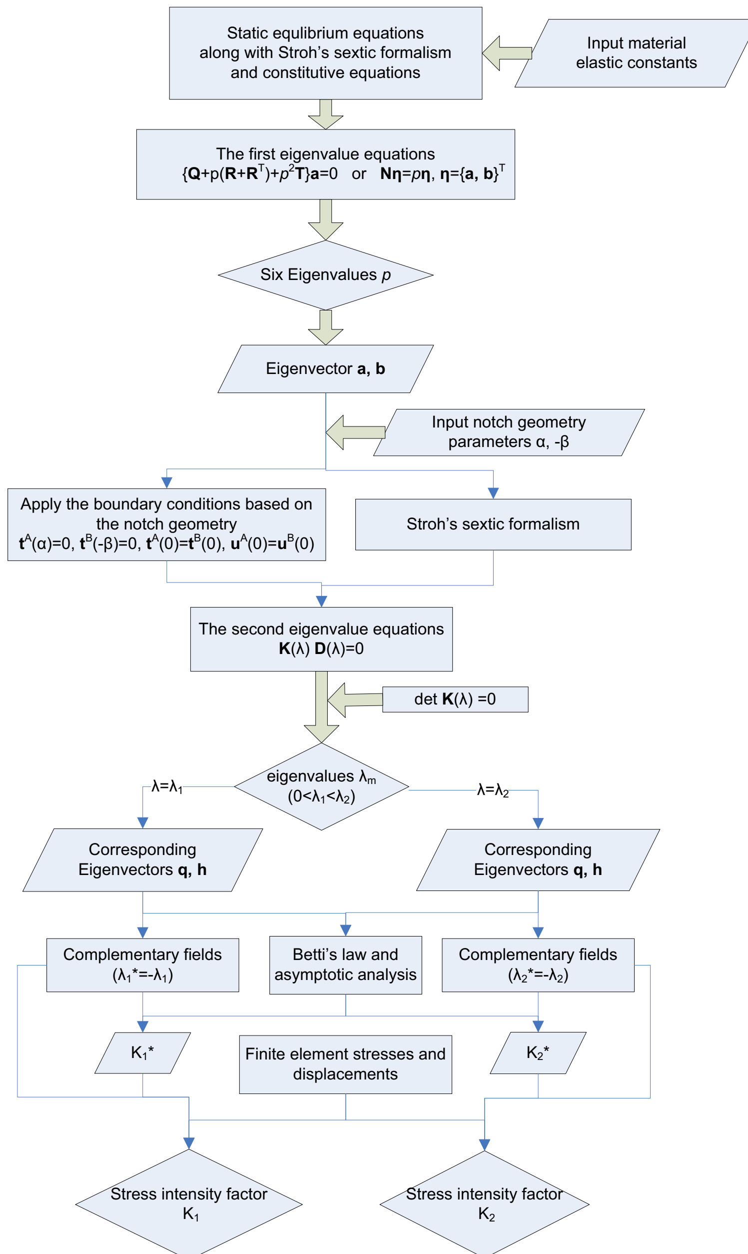

Fig. 2 A flow chart illustrating a procedure to obtain the stress intensity factor

Applications and results

The multi-layered structures considered in our study are shown in Fig. 3. Typical material combinations in microelectronic devices are taken into account. The elastic properties of the materials and the evaluation of λ for various joint geometries and material combinations are listed in

Table 1. Plane strain conditions are assumed in all modelling. Finite element analyses are performed with ABAQUS. Eight-noded isoparametric elements were used. We also assume that the materials are perfectly bonded along the interface. The mesh refinement, dimensions and loading conditions are depicted in Fig. 3. Beam span L, height h and width w of silicon substrate are 10mm, 1mm and 3.4mm, respectively. The anisotropic silicon substrate employed here is 350μm thick oriented in [100] crystal direction with elastic constants of $C_{11} = 165.7GPa$, $C_{12} = 63.9GPa$ and $C_{44} = 79.56GPa$ [13].

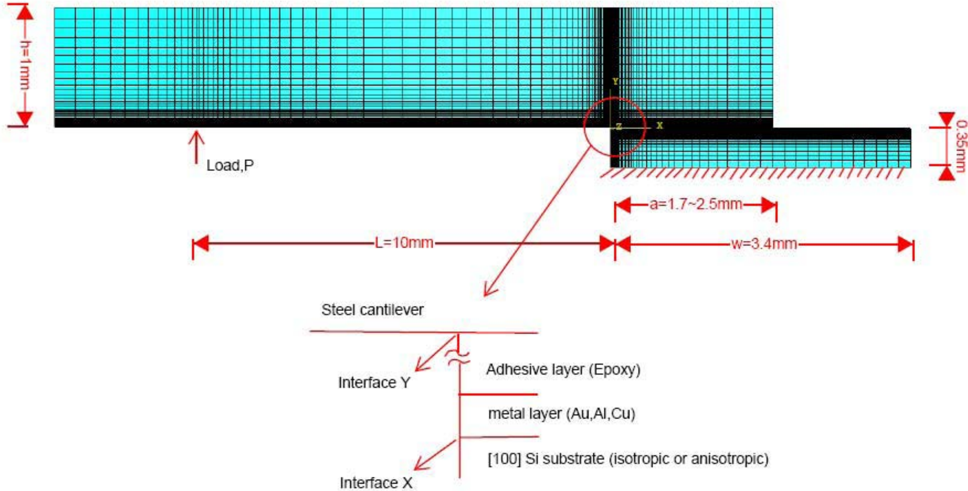

Fig. 3 Specimen geometry, finite element mesh and loading conditions.

Table 1
Material elastic properties and the orders of stress singularities with varying material combinations and joint geometries

	Isotropic Materials					
Materials Elasticity	**Au**	**Cu**	**Al**	**Si**	**Steel**	**Epoxy**
Young's Modulus (GPa)	83	129	70	167	200	2.50
Poisson's Ratio	0.44	0.34	0.35	0.30	0.30	0.30
Interface X	**Material A**	**Material B**	λ_1	**Material A**	**Material B**	λ_1
	Au	Isotropic silicon	0.9332	Au	Anisotropic silicon	0.9522
	Al		0.9304	Al		0.9481
	Cu		0.9912	Cu		0.9967
Interface Y	Steel	Epoxy	0.7049			

Non-dimensional stress intensity factor

A combination of the finite element results and a path independent contour integral is used to evaluate the stress intensity factor. Since K_m^n has the unit of $(stress)(length)^{1-\lambda_m}$, dimensional considerations dictate that

$$Y_m^n\left(\tfrac{a}{w}, \tfrac{t}{t_0}\right) = \frac{K_m^n}{\frac{6PL}{bh^2} w^{1-\lambda}}, \tag{7}$$

where a, w, t, t_0, P, L, b, and h denote, respectively, the bond length, substrate width, conductor layer thickness, nominal thickness, concentrated force, and span, width and height of the steel beam (Fig. 3), whereas Y is a shape function depending on the notch geometry and material elastic constants. Furthermore, we can write

$$Y_m^n\left(\tfrac{a}{w},\tfrac{t}{t_0}\right)=Y_{ref}^n\cdot f\left(\tfrac{a}{w}\right)\cdot g\left(\tfrac{t}{t_0}\right), \tag{8}$$

where

$$f\left(\tfrac{a}{w}\right)=\frac{Y_m^n\left(\tfrac{a}{w},\tfrac{t}{t_0}=0.2\right)}{Y_{ref}^n},\ g\left(\tfrac{t}{t_0}\right)=\frac{Y_m^n\left(\tfrac{a}{w}=0.5,\tfrac{t}{t_0}\right)}{Y_{ref}^n},\ Y_{ref}^n=Y_m^n\left(\tfrac{a}{w}=0.5,\tfrac{t}{t_0}=0.2\right).$$

The results obtained from the H-integral approach can be fitted to the power function $f(geometry)=j(geometry)^k$ and $g(geometry)=l(geometry)^s$. The best-fit values for the isotropic Cu/Si and Au/Si cases are shown in Fig. 4.

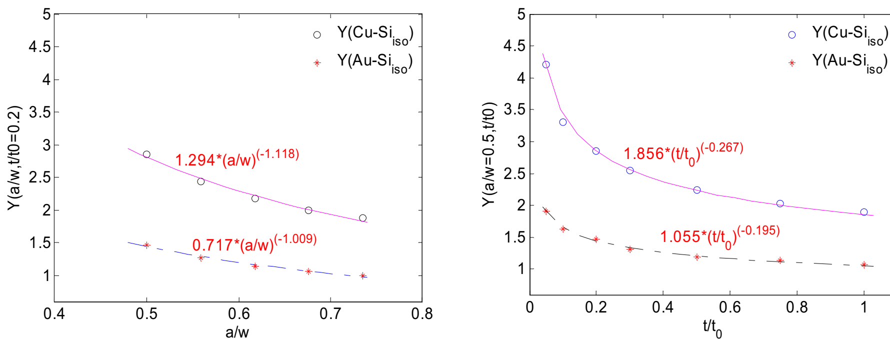

Fig. 4 Non-normalized fitting functions (Cu/Si and Au/Si)

Consequently, standardized numerical formulae for two individual cases read for the isotropic Cu/Si case:

$$Y_{H\text{-integral}}^n\left(\tfrac{a}{w},\tfrac{t}{t_0}\right)=2.854\times0.454\left(\tfrac{a}{w}\right)^{-1.118}\times0.651\left(\tfrac{t}{t_0}\right)^{-0.267},\text{ where } t_0\text{=1000}nm \tag{9}$$

and for the isotropic Au/Si case:

$$Y_{H\text{-integral}}^n\left(\tfrac{a}{w},\tfrac{t}{t_0}\right)=1.464\times0.490\left(\tfrac{a}{w}\right)^{-1.009}\times0.721\left(\tfrac{t}{t_0}\right)^{-0.195},\text{ where } t_0\text{=1000}nm \tag{10}$$

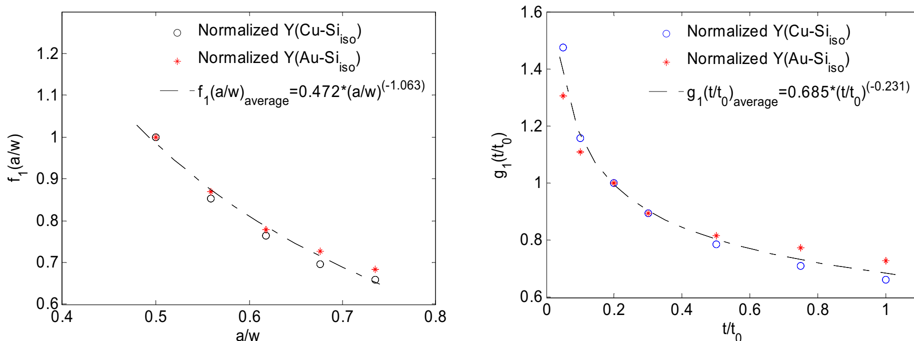

Fig. 5 The power function $f\left(a/w\right)$ and $g\left(t/t_0\right)$ for different material combinations

Furthermore, if we normalize the dimensionless stress intensity factor by dividing with the corresponding reference value, the respective power function for different material combinations

amazingly falls very close to one curve, see Fig. 5. The greatest scatters of two individual cases from the average fitting are 7.8% and 5.6% for Cu/Si and Au/Si case, respectively. It is still appreciable from the engineering's perspective. Hence, the average solution proposed here may be a favourable alternative.

The effect of the bond width, the thickness of the metal layer and the material elasticity

The effect of the bond width is analyzed. The metal layer remains 200nm thick whereas the bond width is varied from 1.7mm to 2.5mm. As expected, the stress intensity factor clearly decreases for the free edge interface (Interface X) with the bond width but change insignificantly for the 90° sharp notch (Interface Y.).

In addition, the effect of the elastic mismatch on the mode I stress intensity factor is also investigated. Alternative conductor layers of copper (Cu), gold (Au) or aluminium (Al) are employed for the analysis as material A, see Fig. 1. For Interface X, it can be observed from Fig. 6 that the structure with a Cu layer yields the highest dimensionless stress intensity factor Y_1^n, followed by that with Au and Al layer. A comparison between isotropic Si and anisotropic Si substrate is also included. Anisotropy of the Si substrate has a significant influence on the stress intensity factor when combined with an Au or Al metal layer but not with a Cu layer. Unlike the response of the structure with a Cu layer, the other two metal materials combined with an isotropic Si substrate produce lower values of the stress intensity factor than those combined with an anisotropic Si substrate. By contrast, the influence of material anisotropy on interface normal stresses is shown in Fig. 7. It is shown that the material isotropy generates the high interface stresses for all specimens. The specimen with a 200nm thick and 2.1mm wide Cu layer produces a lower driving force than for a specimen with an Au or an Al layer if subjected to the same load.

The effect of thin-film thickness on the dimensionless stress intensity factor is further explored. In these simulations, the bond area is kept constant ($a = 1.7\text{mm}$), the thin-film thickness equal to 50, 100, 200, 300, 500, 750 and 1000 nm are analyzed. It turns out that the magnitude of stress intensity factor for Interface X approaches a constant value with the increase of the thickness of metal layer. The dimensionless stress intensity factor is sensitive to thin-film cases whereas the thickness component can be ignored when a metal layer is above 300 nm thick.

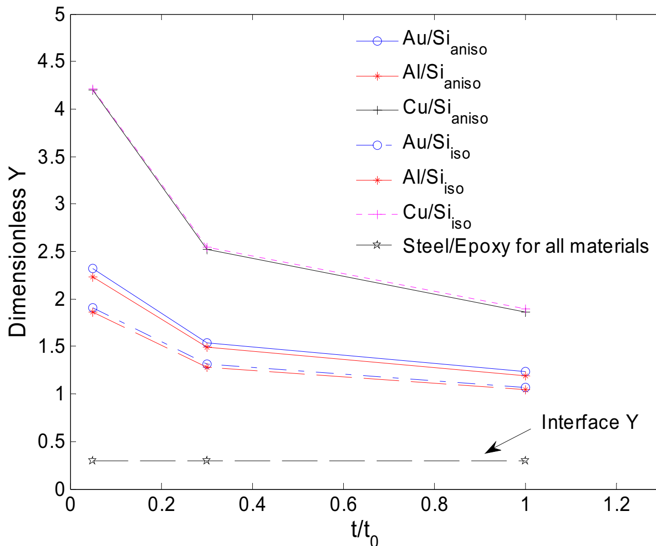

Fig. 6 The effect of material properties and metal layer thickness at Interface X and Interface Y

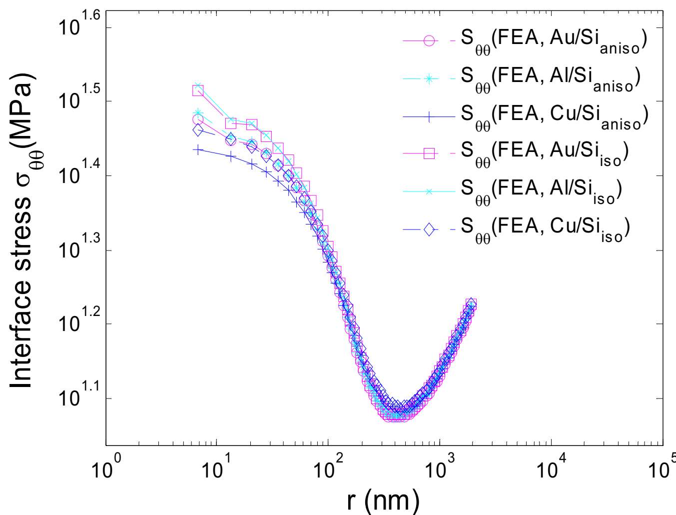

Fig. 7 The effect of the material anisotropy on interface normal stress

Discussion: Applicability of H-integral approach

The proposed H-integral approach is based on the assumption of elasticity with the dominance of a K-field. Consider a typical case for an Au layer bonded with an isotropic silicon substrate. The interface stress component $\sigma_{\theta\theta}$ is plotted against the distance from the free edges with varying metal layer thickness (Fig. 8a) and various bond width (Fig. 8b). The extent of the K-dominated region is estimated by comparing finite element results with asymptotic analysis. The two solutions are in good agreement for all the cases. It matches up to a radial distance of 70nm for the specimen with a 1.7mm wide and 300nm thick metal layer regarding a 5% deviation. It matches up to 45nm for the specimen with a 200nm thick and 2.5mm wide metal layer considering a 10% difference. As expected, the thicker the thin-film layer, the greater is the valid K-dominated region. Within the bond range we investigated here, the difference of K-field has not a significant dependence on the bond width. It seems that the deviation is slightly larger with increasing bond width but tends to stabilize for the specimens with a bond width larger than 2.3mm. Moreover, the use of the critical stress intensity factor as a failure initiation parameter requires that the size of inelastic zone (process zone) should be much smaller than the extent of the K-field under the failure load. Taking Au(200nm)/Si as an example and assuming the elastic–linear hardening model with a yield stress of $160MPa$ and a hardening modulus of 8.3 GPa. Applying the critical delamination load $P_c = 0.6N$ [3] to the specimen, it was observed that no plastic strain occurred in the finite element analysis.

Summary

A feasible H-integral approach to compute the edge stress intensity factor in multi-layered structural components with weak singularities is shown in the present work. The computational procedure is illustrated in a flow chart. Standardized numerical formulae for varying material combinations are proposed from a design engineer's perspective. It has also been shown that the material dependence can be normalized. The effects of bond width, elastic mismatch and metal layer thickness on the stress intensity factor have been quantified. Influence of anisotropy of single crystal silicon on the stress intensity factor and the interface stress is also represented. Lastly, the

applicability of the H-integral approach has been checked. The extent of the K-dominated field is assessed by comparing the asymptotic solution to the detailed finite element analysis. It is observed that the valid range of the K-field is strongly influenced by thin-film thickness but not by bond width.

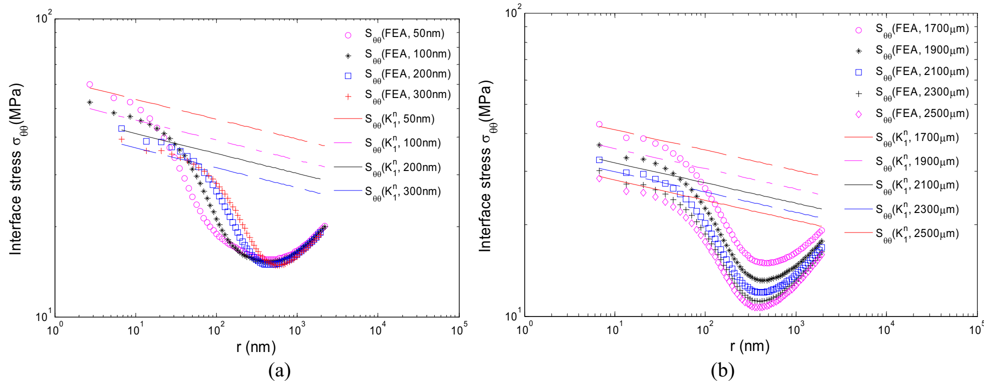

Fig. 8 K-dominated field for specimens with (a) an Au layer thickness from 50 to 300nm and (b) an Au layer bond width from 1.7mm to 2.5mm

References

[1] T. Kitamura, T. Shibutani and T. Ueno: Engineering Fracture Mechanics Vol. 69 (2002), p. 1289

[2] T. Kitamura, H. Hirakata and T. Itsuji: Engineering Fracture Mechanics Vol. 70 (2003), p. 2089

[3] T. Kitamura, H. Hirakata and D. Van Truong: Thin Solid Films Vol. 515 (2007), p. 3005

[4] L.Y. Shang, Z.L. Zhang and B. Skallerud: Engineering Fracture Mechanics Vol. 75 (2008), p. 1064

[5] L.Y. Shang, Z.L. Zhang and B. Skallerud: Submitted (2008).

[6] T.C.T. Ting, in: *Anisotropic Elasticity: Theory and Applications*, Oxford University Press, NY (1996).

[7] P.E.W. Labossiere and M.L. Dunn: Engineering Fracture Mechanics Vol. 62 (1999), p. 555

[8] A.N. Stroh: Philosophical Magazine Vol. 3 (1958), p.625

[9] M.L. Williams: Journal of Applied Mechanics Vol. 19 (1952), p. 526

[10] D.B. Bogy and K.C. Wang: International Journal of Solids and Structures, Vol. 7 (1971), p. 993

[11] G.L. Rogers and M.L: Causey: *Mechanics of engineering structures,* John Wiley and Sons, NY (1962.).

[12] T.C.T. Ting: Damage and Failure of Interfaces, Rossmanith (ed.), Balkema, Rotterdam, (1998), p. 75

[13] W.P. Mason: *Physical acoustics and properties of solids*, New York, Van Nostrand (1958).